

This is the accepted version of the following document:

L. Leyva, D. Castanheira, A. Silva and A. Gameiro, "Quasi-Orthogonal SFBC for Monostatic MIMO ISAC Scenarios," 2022 13th International Symposium on Communication Systems, Networks and Digital Signal Processing (CSNDSP), 2022, pp. 305-309, doi: 10.1109/CSNDSP54353.2022.9907913.

© 2022 IEEE. Personal use of this material is permitted. Permission from IEEE must be obtained for all other uses, in any current or future media, including reprinting/republishing this material for advertising or promotional purposes, creating new collective works, for resale or redistribution to servers or lists, or reuse of any copyrighted component of this work in other works.

# Quasi-Orthogonal SFBC for Monostatic MIMO ISAC Scenarios

Leonardo Leyva  
*Instituto de  
Telecomunicações and  
University of Aveiro*  
Aveiro, Portugal  
leoleval@av.it.pt

Daniel Castanheira  
*Instituto de  
Telecomunicações*  
Aveiro, Portugal  
dcastanheira@av.it.pt

Adão Silva  
*Instituto de  
Telecomunicações and  
University of Aveiro*  
Aveiro, Portugal  
asilva@av.it.pt

Atilio Gameiro  
*Instituto de  
Telecomunicações and  
University of Aveiro*  
Aveiro, Portugal  
amg@ua.pt

**Abstract**— This paper studies the performance of the quasi-orthogonal Tirkkonen spatial-frequency block code (SFBC) for integrated sensing and communication (ISAC) scenarios. The considered scenario is a MIMO monostatic ISAC base station (BS), where transmitter and radar antenna arrays are co-located enabling the virtual array concept. The quasi-orthogonal Tirkkonen SFBC is encapsulated in an OFDM waveform, the radar processing is performed over the resulting OFDM frame. The performance in terms of radar and communication metrics of Tirkkonen SFBC is presented and compared with orthogonal Alamouti SFBC and the spectrally interleaved waveform approach, widely used in radar-like scenarios. The resulting Mean Square Error (MSE) of the Angle of Arrival (AoA) is chosen as the radar metric while the bit-error-rate (BER) is used to present the communication performance. The results show that Tirkkonen is a good candidate for future ISAC scenarios.

**Keywords**—ISAC, SFBC, Virtual Array, MIMO, Tirkkonen

## I. INTRODUCTION

Integrated sensing and communication (ISAC) systems have attracted increased interest in recent years [1-4]. The possibilities offered by this paradigm, namely improved spectral/energy efficiency, hardware infrastructure savings and possible foreseen applications (e.g., smart cities, Internet of Things (IoT) and intelligent transportation systems (ITS)) have led to consider this paradigm as a feature of the physical layer (PHY) for 6G and future WiFi standards.

There are many proposals in the literature concerning stand-alone ISAC systems, with a single base station (BS) performing communication and radio-sensing capabilities [2, 5-6]. For instance, in [2] communication waveforms are considered, while in [6] the focus is the use of radar waveforms for dual functionality systems. On the other hand, other contribution centers on ISAC networking paradigms [3, 7]. For instance, [3] describes an ultra-dense network (UDN), where the massive level of cooperation allows to jointly provide both communication and radio-sensing capabilities being the concept of multistatic radar key for enabling radio-sensing applications. On the other hand, [7] presents a “perceptive mobile network” paradigm, which concentrates

on the topologies that such a network may support for radio-sensing. Also, it introduces the foreseen required modification in terms of signaling and how the different channels of 5G can be exploited for radio-sensing. Both stand-alone and networking agree that multiple-input multiple-output (MIMO) and orthogonal frequency division multiplexing (OFDM) are enabler technologies in developing future ISAC systems.

MIMO has been extensively deployed for wireless communication systems, which brings diversity, array and spatial multiplexing gains. These possibilities enhance the performance in terms of capacity, link reliability and coverage. On the other hand, MIMO is also a reality for the radar community [8-10]. MIMO radar has shown several benefits when compared with the classical phased array radar, like enhanced flexibility concerning the waveform design and higher resolution [11]. More specifically, when the transmitting and receiving array antennas are co-located, a virtual array with a higher antenna aperture can be exploited. This is possible using a specific antenna spacing and a set of orthogonal waveforms [11]. Besides, [11] shows that the Cramér-Rao bound (CRB) of target parameter estimation is minimized when orthogonal probing signals are employed.

The orthogonality between the probing beams can be achieved through spectrally interleaved OFDM [12], which enables communication and radar functionalities. However, this waveform gets no diversity and presents low spectral efficiency. The transmission of several replicas of the symbols encoded in space-frequency is a technique known as space-frequency block codes (SFBC) [13]. SFBCs bring diversity to the system but still permit exploiting the enhanced aperture size of the virtual array in a co-located MIMO radar topology. In this regard, [13] discussed a technique to exploit the diversity provided by the STBC codes for secure radar imaging applications. More recently, the contribution in [14] discussed the exploitation of Alamouti SFBC for the ISAC monostatic paradigm, where the results showed the suitability of this code for radio-sensing purposes. This result was extended to a general framework regarding orthogonal SFBC codes in [15], where Alamouti was compared to Tarokh in terms of radio-sensing and communication. The latter contribution showed that although Tarokh presents better resolution than Alamouti for radio-sensing, it also reports reduced unambiguous range, which can be catastrophic when ranging objects on the edge of the desired exploration zone.

---

This work has received funding from the European Union’s Horizon 2020 research and innovation programme under the Marie Skłodowska-Curie ETN TeamUp5G, grant agreement No. 813391.

This is because the unambiguous range is inverse to the number of resources used by the SFBC in the frequency domain, i.e., the Tarokh code employs a frequency block with eight sub-carriers, while Alamouti uses only two sub-carriers [15].

This work evaluates the performance of Tirkkonen SFBC [16] in a joint radio-sensing and communication scenario. Tirkkonen is a quasi-orthogonal SFBC with a unitary rate, i.e., uses the same number of sub-carriers and transmitting antennas. This allows obtaining two times the unambiguous range compared to four-antenna orthogonal SFBC with half rate, (e.g., Tarokh). Then, the enhanced unambiguous range enables ranging targets at twice the distance. However, the probing signals are not orthogonal but quasi-orthogonal. Therefore, we evaluate the effect of the interference in a joint radio-sensing and communication scenario. More specifically, we consider a monostatic MIMO-OFDM ISAC BS that jointly communicates with user equipment and detects a target. The performance of the Tirkkonen SFBC is evaluated for communication and radio-sensing functionalities. For radio-sensing, the metrics are the resolution and Mean Square Error (MSE) obtained in the estimation of the angle-of-arrival (AoA), and the bit-error-rate (BER) is considered for the communication.

To summarize, the major contributions of this paper are:

- Integration of communication and radio-sensing functionalities in a single platform is achieved using a quasi-orthogonal SFBC.
- Evaluation of the interference introduced by the quasi-orthogonal SFBC in the performance of the radio-sensing component.
- Comparison between Tirkkonen SFBC, spectrally interleaved waveform and Alamouti SFBC in terms of radio-sensing and communication.

The remainder of this paper is organized as follows: Section II introduces the system model, the communication receiver configuration and the radio-sensing signal processing method used for the estimation of parameters. Section III is devoted to discussing the performance results. Finally, section IV concludes the paper.

## II. SYSTEM MODEL

This work considers a scenario with one BS communicating with one user equipment (UE) and sensing the environment, see Fig. 1.

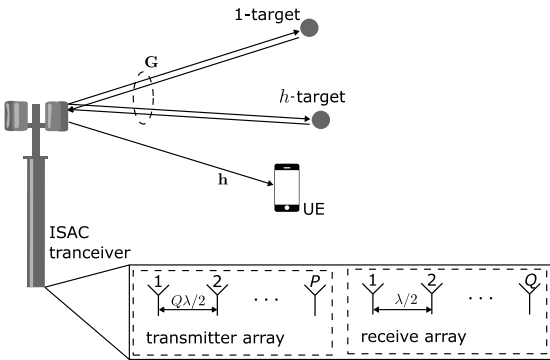


Fig. 1. MIMO-OFDM monostatic ISAC scenario.

At the ISAC BS, the transmitter and receiver uniform linear arrays (ULA) are co-located, i.e., monostatic radar architecture. In Fig. 1, the channel between the BS and UE is represented by the complex vector  $\mathbf{h}$ , and the radar channel by the complex channel matrix  $\mathbf{G}$ .

In the following, for communication purposes, it is considered that the channel was previously estimated, and it is perfectly known by the UE. Besides, for radar processing is considered that the transmitted signal is known by the radar receiver, which is valid since the transmitter and receiver are co-located. The BS is equipped with  $P$  and  $Q$  transmitting and receiving antennas, respectively. The  $P$  transmitting elements are spaced by a distance of  $Q\lambda/2$ , where  $\lambda$  denotes the wavelength. The specific spacing of the transmitting antennas obeys the virtual array concept [11], which enhance the attained angular resolution [14, 15].

### A. Transmitter

Fig. 2 presents the block diagram for the transmitter branch of the BS. The  $P$  antennas transmit quasi-orthogonal encoded OFDM symbols. In the following, without loss of generality, the Tirkkonen SFBC [16] will be considered. For this SFBC the data rate is unitary and four antennas ( $P=4$ ) are used.

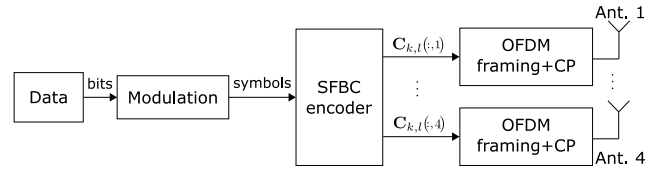


Fig. 2. Block diagram of an ISAC transmitter.

Before the SFBC encoder, the binary data is modulated into a sequence of symbols, the symbols are divided into four streams and coded in space and frequency, according to the matrix

$$\mathbf{C}_{k,l} = \begin{bmatrix} \mathbf{c}_1(k,l) & \mathbf{c}_2(k,l) & \mathbf{c}_3(k,l) & \mathbf{c}_4(k,l) \\ -\mathbf{c}_2^*(k,l) & \mathbf{c}_1^*(k,l) & -\mathbf{c}_4^*(k,l) & \mathbf{c}_3^*(k,l) \\ \mathbf{c}_3(k,l) & \mathbf{c}_4(k,l) & \mathbf{c}_1(k,l) & \mathbf{c}_2(k,l) \\ -\mathbf{c}_4^*(k,l) & \mathbf{c}_3^*(k,l) & -\mathbf{c}_2^*(k,l) & \mathbf{c}_1^*(k,l) \end{bmatrix}, \quad (1)$$

where the columns represent the symbols transmitted by each of the antennas,  $k \in \{0, \dots, N-1\}$  stands for the block subcarrier index, with  $N = N_c/4$  and  $N_c$  the total number of sub-carriers,  $l \in \{0, \dots, L-1\}$  represents the OFDM symbol index in an OFDM frame with  $L$  symbols. Finally, for each antenna, the OFDM framing and cyclic prefix (CP) adding operations follows.

### B. User equipment terminal

The UE is equipped with a single antenna, and the channel  $\mathbf{h}$  between the four transmitting antenna elements and the single receiver element, as pointed out, is perfectly known. The objective is to recover the communication original data transmitted from the BS. Fig. 3 introduces the receiver

diagram of the UE. First, the CP is removed and the received signal deframed, then the symbols are decoded by the SFBC Tirkkonen decoding block, which follows the data estimate.

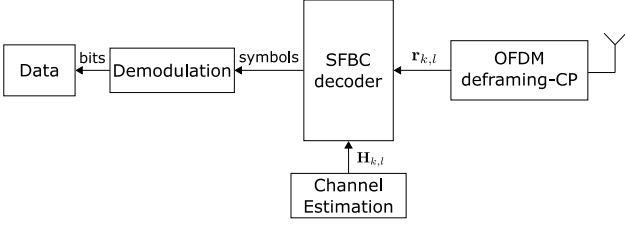


Fig. 3. Block diagram of the receiver in the UE.

After OFDM deframing, CP removal, and considering that the coherence bandwidth is equal or greater than the bandwidth of a sub-carrier block (i.e., four consecutive sub-carriers for Tirkkonen SFBC), the received signal at the UE for the  $k$  th index frequency block and  $l$  th OFDM symbol, can be expressed as [15],

$$\mathbf{r}_{k,l} = \mathbf{C}_{k,l} \mathbf{h}_{k,l} + \mathbf{n}_{k,l} \quad (2)$$

where,  $\mathbf{h}_{k,l}$  is the channel frequency response between the four transmitting antennas and the single receiving antenna and  $\mathbf{n}_{k,l} \sim \mathcal{CN}(\mathbf{0}, N_0 \mathbf{I})$  denotes white Gaussian noise.

The soft decision of the transmitted data vector  $\mathbf{c}_{k,l} = [\mathbf{c}_1(k,l) \ \mathbf{c}_2(k,l) \ \mathbf{c}_3(k,l) \ \mathbf{c}_4(k,l)]^T$  can be obtained by,

$$\tilde{\mathbf{c}}_{k,l} = \mathbf{W}_{k,l} \bar{\mathbf{r}}_{k,l} \quad (3)$$

where  $\mathbf{W}_{k,l} = (\mathbf{H}_{k,l}^H \mathbf{H}_{k,l} + N_0 \mathbf{I})^{-1} \mathbf{H}_{k,l}^H$  stands for the Mean Minimum Square Error (MMSE) equalizer,  $\bar{\mathbf{r}}_{k,l}$  represents the equivalent received signal, whose structure is given by,

$$\bar{\mathbf{r}}_{k,l} = \mathbf{H}_{k,l} \mathbf{c}_{k,l} + \mathbf{n}_{k,l}, \quad (4)$$

and  $\mathbf{H}_{k,l}$  denotes the equivalent channel matrix, for Tirkkonen SFBC, which is given by [16],

$$\mathbf{H}_{k,l} = \begin{bmatrix} \mathbf{h}_1(k,l) & \mathbf{h}_2(k,l) & \mathbf{h}_3(k,l) & \mathbf{h}_4(k,l) \\ \mathbf{h}_2^*(k,l) & -\mathbf{h}_1^*(k,l) & \mathbf{h}_4^*(k,l) & -\mathbf{h}_3^*(k,l) \\ \mathbf{h}_3(k,l) & \mathbf{h}_4(k,l) & \mathbf{h}_1(k,l) & \mathbf{h}_2(k,l) \\ \mathbf{h}_4^*(k,l) & -\mathbf{h}_3^*(k,l) & \mathbf{h}_2^*(k,l) & -\mathbf{h}_1^*(k,l) \end{bmatrix}. \quad (5)$$

### C. RADAR processing

As pointed out, the radar functionality is performed in the ISAC transceiver, co-located with the transmitter. Fig. 4 shows the scheme of the radar signal processing. The receiver ULA is equipped with  $Q$  antenna elements separated by  $\lambda/2$ . The estimation of parameters (e.g., range, angle and

velocity) of the objects in the surrounding is performed by the radar processing illustrated in Fig. 4.

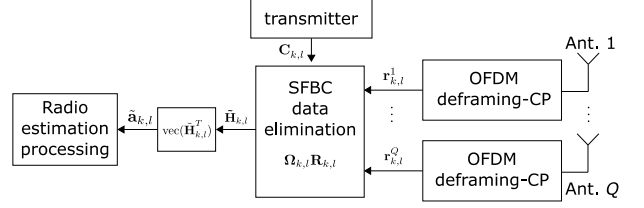


Fig. 4. Radar receiver representation of the co-located MIMO-ISAC BS.

Following OFDM deframing and CP removal, the received signal for the  $k$  th sub-carrier block and  $l$  th OFDM symbol at the  $q$  th received antenna can be described by [15],

$$\mathbf{r}_{k,l}^q = \mathbf{C}_{k,l} \mathbf{g}_{k,l}^q + \mathbf{n}_{k,l}^q \quad (6)$$

where  $\mathbf{g}_{k,l}^q$  is the channel frequency response between the four transmitting antennas and the  $q$  th antenna element of the receiver ULA and  $\mathbf{n}_{k,l} \sim \mathcal{CN}(\mathbf{0}, N_0 \mathbf{I})$  denotes white Gaussian noise.

From (6), we can define the complex matrices  $\mathbf{G}_{k,l} = [\mathbf{g}_{k,l}^1, \dots, \mathbf{g}_{k,l}^Q]$ ,  $\mathbf{R}_{k,l} = [\mathbf{r}_{k,l}^1, \dots, \mathbf{r}_{k,l}^Q]$  and  $\mathbf{N}_{k,l} = [\mathbf{n}_{k,l}^1, \dots, \mathbf{n}_{k,l}^Q]$  as the concatenation of the received signals in the  $Q$  antennas, from which follows,

$$\mathbf{R}_{k,l} = \mathbf{C}_{k,l} \mathbf{G}_{k,l} + \mathbf{N}_{k,l} \quad (7)$$

The channel matrix  $\mathbf{G}_{k,l}$  is the superposition of  $H$  reflections from objects within the surrounding, it can be modelled by,

$$\mathbf{G}_{k,l} = \sum_{h=1}^H \mathbf{a}_{tx}(\theta_h) \mathbf{a}_{rx}^T(\theta_h) e^{j2\pi T_0 f_{Dh} l} e^{-j2\pi \Delta f \tau_h k} \quad (8)$$

where  $\tau = 2R/c_0$  denotes the delay,  $f_D = 2v/\lambda$  is the Doppler frequency shift,  $T_0$  stands as the overall OFDM symbol duration,  $\phi = \sin(\theta)$  is the angle,  $\Delta f$  represents the subcarrier separation and  $c_0$  is the speed of the light. While  $\mathbf{a}_{rx}(\theta)$  and  $\mathbf{a}_{tx}(\theta)$  are the receiver and transmitter array response vectors, respectively. Like [15], the  $p$  th element position of the vector  $\mathbf{a}_{k,l} = \text{vec}(\mathbf{G}_{k,l}^T)$ , can be represented as,

$$\mathbf{a}_{k,l}(p) = \sum_{h=1}^H e^{-j\pi p \phi} e^{j2\pi T_0 f_{Dh} l} e^{-j2\pi \Delta f \tau_h k} \quad (9)$$

The estimate of the channel matrix  $\mathbf{G}_{k,l}$  is obtained by equalizing the received signal  $\mathbf{R}_{k,l}$  like,

$$\tilde{\mathbf{G}}_{k,l} = \mathbf{\Omega}_{k,l} \mathbf{R}_{k,l} \quad (10)$$

Where  $\mathbf{\Omega}_{k,l}$  is the equalizer matrix, which is based on the transmitted signal in (1). For instance, for the MMSE equalizer  $\mathbf{\Omega}_{k,l}^{MMSE} = (\mathbf{C}_{k,l}^H \mathbf{C}_{k,l} + N_0 \mathbf{I})^{-1} \mathbf{C}_{k,l}^H$ . Therefore, from  $\tilde{\mathbf{G}}_{k,l}$  follows  $\tilde{\mathbf{a}}_{k,l} = \text{vec}(\tilde{\mathbf{G}}_{k,l}^T)$ , where entry  $p$  is  $\tilde{\mathbf{a}}_{k,l}(p)$ . The channel response is equivalent to the channel response of a system with one transmitting antenna and a uniform linear array with  $4Q$  receiving antennas with a separation between antennas of  $\lambda/2$ . This  $4Q$ -element array is the virtual antenna array [11], which is obtained with just  $4+Q$  physical antenna elements. Then, from (9), the parameters of the targets (i.e., velocity, range and angle of arrival) can be estimated by performing a IDFT or DFT along the three dimensions  $(k, l, p)$  of  $\tilde{\mathbf{a}}_{k,l}(p)$  [17]. The DFT over the dimension  $l$  returns and estimate of the velocity, an IDFT over  $k$  gives the estimative of the range and the IDFT over  $p$  gives the angle of arrival of the target.

### III. SYSTEM PERFORMANCE

In this section, the performance of the Tirkkonen SFBC for the ISAC monostatic scenario is presented. The performance is evaluated for radar and communication functionalities. For radar, the metrics are the attained resolution and the MSE of the AoA's estimate, while for communication the BER is considered.

#### A. Scenario description

The considered carrier frequency is 24 GHz. The waveform is OFDM, the parameters of the waveform have been chosen to fulfil a set of design criteria as, maximum unambiguous range  $r_{unamb}$ , and maximum unambiguous velocity  $v_{unamb}$ . The radar estimate is performed over an OFDM frame with 64 sub-carriers and 8 OFDM symbols. The MSE and BER curves are obtained through Monte Carlo simulations, considering 40000 OFDM symbols, which gives 5000 radar estimates. The design criteria and OFDM parameters are summarized in Table I.

TABLE I. OFDM AND DESIGN CRITERIA PARAMETERS FOR ISAC SYSTEM.

Parameters	Value
Bandwidth $B$	48.78 MHz
Maximum unambiguous range $r_{unamb}$	300 m
Maximum unambiguous velocity $v_{unamb}$	43.75 m/s
Number subcarriers $N_c$	64
Subcarrier spacing $\Delta f$	76.230 kHz
Cyclic prefix duration $\tau_{CP}$	1 $\mu$ s
Total OFDM symbol duration $T_0$	14.12 $\mu$ s

#### B. Performance results

Fig. 5 shows a comparison of the attained AoA resolution between SFBCs Tirkkonen, Alamouti and the spectrally interleaved waveform approach presented in [12].

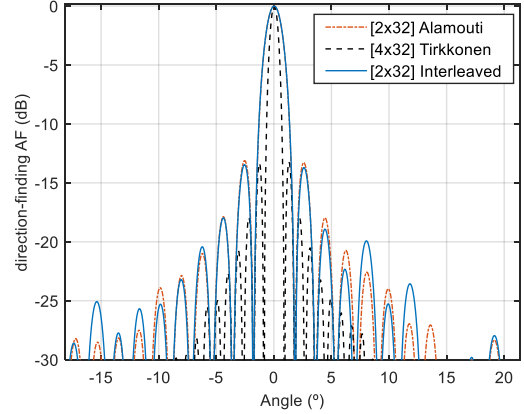


Fig. 5. Direction-finding resolution comparison between SFBCs Tirkkonen, Alamouti and spectrally interleaved waveform for a target located at  $0^\circ$  at high SNR regime ( $E_b/N_0 = 8$  dB).

As it can be observed, Tirkkonen presents better AoA resolution and low side-lobe level when compared to Alamouti and the spectrally interleaved waveform, which present similar AoA resolution and side-lobe levels. Therefore, we can say that the interference resulting from the quasi-orthogonality of Tirkkonen SFBC does not have a relevant impact on the AoA resolution at a high SNR regime.

Fig. 6 presents the MSE curves obtained for Tirkkonen SFBC (for Maximum Ratio Combining (MRC) and MMSE equalizers), Alamouti and the spectrally interleaved waveform.

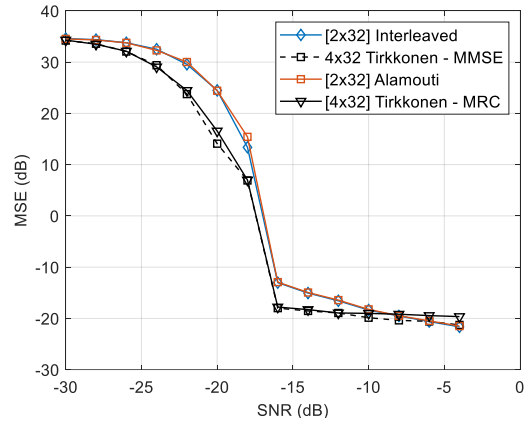


Fig. 6. Comparison of the MSE of the AoA between Tirkkonen, Alamouti and spectrally interleaved waveform.

From Fig. 6, it can be noted that the Tirkkonen – MMSE scheme reports the best overall performance. Also, the spectrally interleaved waveform and Alamouti present similar performance and converge for the performance obtained with Tirkkonen MMSE after  $\text{SNR} = -8$  dB. Besides, Tirkkonen – MMSE presents and slightly better performance than Tirkkonen – MRC, which is more evident from SNR greater

than -8 dB. Finally, Fig. 7 illustrates the obtained BER for Tirkkonen, Alamouti and the spectrally interleaved waveform [12].

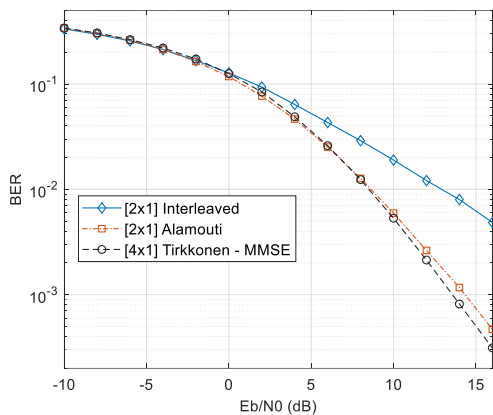


Fig. 7. BER performance comparison.

Fig. 7 shows that the quasi-orthogonal Tirkkonen SFBC (MMSE equalizer) outperforms the orthogonal 2x1 Alamouti SFBC and the spectrally interleaved waveform since the diversity order is higher than 2. Therefore, the quasi-orthogonal Tirkkonen SFBC can be seen as a promising candidate for the integration of radio-sensing and communications functionalities. Although the quasi-orthogonality, it was shown that the structure of the Tirkkonen SFBC signals allows the formation of virtual arrays, achieving a similar performance of Alamouti and spectrally interleaved orthogonal signaling while enabling diversity in the communication domain. Besides, it presents an unambiguous range of 3.22 us, which is twice the obtained for Tarokh SFBC in [15].

#### IV. CONCLUSIONS

This paper evaluates the performance of quasi-orthogonal Tirkkonen SFBC for the future integration of radio-sensing and communication functionalities. The quasi-orthogonality properties provided a similar performance to those obtained with orthogonal signaling. As with orthogonal signals, this enhances the radar resolution significantly by resorting to the virtual array concept. Regarding the communication functionality, Tirkkonen presents more diversity than Alamouti and the spectrally interleaved approach, reducing the resulting BER. Therefore, for integrated sensing and communication systems, the use of quasi-orthogonal SFBC is preferred over orthogonal Alamouti SFBC and spectrally interleaved waveform.

#### REFERENCES

- [1] M. Giordani, M. Polese, M. Mezzavilla, S. Rangan and M. Zorzi, "Toward 6G Networks: Use Cases and Technologies," *IEEE Commun Mag.*, vol. 58, no. 3, pp. 55-61, March 2020.
- [2] F. Liu, C. Masouros, A. P. Petropulu, H. Griffiths and L. Hanzo, "Joint Radar and Communication Design: Applications, State-of-the-Art, and the Road Ahead," *IEEE Trans Commun.*, vol. 68, no. 6, pp. 3834-3862, June 2020.
- [3] L. Leyva, D. Castanheira, A. Silva, A. Gameiro and L. Hanzo, "Cooperative Multiterminal Radar and Communication: A New

- Paradigm for 6G Mobile Networks," *IEEE Veh. Technol. Mag.*, vol. 16, no. 4, pp. 38-47, Dec. 2021
- [4] A. Gameiro, D. Castanheira, J. Sanson and P. Monteiro, "Research challenges, trends and applications for future joint radar communications systems," *Wirel. Pers. Commun.*, vol. 100, no. 1, pp. 81-96, March 2018.
- [5] B. Paul, A. R. Chiriyath and D. W. Bliss, "Survey of RF communications and sensing convergence research," *IEEE Access*, vol. 5, pp. 252-270, 2017.
- [6] A. Hassanien, M. G. Amin, Y. D. Zhang and F. Ahmad, "Dual-Function Radar-Communications: Information Embedding Using Sidelobe Control and Waveform Diversity," *IEEE Trans. Signal Process.*, vol. 64, no. 8, pp. 2168-2181, April 15, 2016.
- [7] A. Zhang, M. L. Rahman, X. Huang, Y. J. Guo, S. Chen and R. W. Heath, "Perceptive Mobile Networks: Cellular Networks With Radio Vision via Joint Communication and Radar Sensing," *IEEE Veh. Technol. Mag.*, vol. 16, no. 2, pp. 20-30, June 2021.
- [8] E. Fishler, A. Haimovich, R. Blum, D. Chizhik, L. Cimini and R. Valenzuela. MIMO radar: an idea whose time has come. Proceeding of the 2004 IEEE Radar Conference, Philadelphia, PA, USA, 29-29 April 2004; pp. 71-78. doi: 10.1109/NRC.2004.1316398.
- [9] F. Liu, C. Masouros, A. Li, H. Sun and L. Hanzo. MU-MIMO Communications With MIMO Radar: From Co-Existence to Joint Transmission. *IEEE Trans. Wirel. Commun.* 2018, 17, pp. 2755-2770. doi: 10.1109/TWC.2018.2803045.
- [10] W. Roberts, P. Stoica, J. Li, T. Yardibi and F. A. Sadjadi. Iterative Adaptive Approaches to MIMO Radar Imaging. *IEEE J. Sel. Top. Signal Process.* 2010, 4, pp. 5-20. doi: 10.1109/JSTSP.2009.2038964.
- [11] J. Li and P. Stoica. MIMO Radar with Colocated Antennas. *IEEE Signal Process. Mag.* 2007, 5, pp. 106-114. doi: 10.1109/MSP.2007.904812.
- [12] J. B. Sanson, D. Castanheira, A. Gameiro and P. P. Monteiro. Cooperative Method for Distributed Target Tracking for OFDM Radar With Fusion of Radar and Communication Information. *IEEE Sens. J.* 2021, 21, pp. 15584-15597. doi: 10.1109/JSEN.2020.3033767.
- [13] A. Sadeque, T. Ali, M. Saquib and M. Ali, "Waveform Transmission Scheme for MIMO Radar Imaging Based on Space-Time Block Codes," *IEEE Trans Aerosp Electron Syst.*, vol. 50, no. 1, pp. 777-785, January 2014.
- [14] L. Leyva, J. Maciel, D. Castanheira, A. Silva and A. Gameiro, "Alamouti coding scheme and virtual array concept for joint radar and communication systems," 2020 12th International Symposium on Communication Systems, Networks and Digital Signal Processing (CSNDSP), 2020, pp. 1-5.
- [15] Leyva L, Costa S, Castanheira D, Silva A, Gameiro A. On SFBC Schemes for Enabling Virtual Array Concept in Monostatic ISAC Scenarios. *Sensors*. 2022; 22(3):1103.
- [16] O. Tirkkonen, A. Boariu and A. Hottinen, "Minimal non-orthogonality rate 1 space-time block code for 3+ Tx antennas," *Proceeding of ISSTA 2000*, pp. 429-432 vol.2, Sept 2000.
- [17] C. Sturm and W. Wiesbeck, "Waveform design and signal processing aspects for fusion of wireless communications and radar sensing," *Proc. IEEE*, vol. 99, no. 7, pp. 1236-1259, July 2011.